

Nearly-Perfect Non-Magnetic Invisibility Cloaking: Analytic Solutions and Parametric Studies

Giuseppe Castaldi,¹ Ilaria Gallina,^{1,2} and Vincenzo Galdi^{1,*}

¹*Waves Group, Department of Engineering, University of Sannio, I-82100 Benevento, Italy*

²*Department of Environmental Engineering and Physics, University of Basilicata, I-85100 Potenza, Italy*

(Dated: September 8, 2021)

Coordinate-transformation approaches to invisibility cloaking rely on the design of an anisotropic, spatially inhomogeneous “transformation medium” capable of suitably re-routing the energy flux around the region to conceal without causing any scattering in the exterior region. It is well known that the inherently magnetic properties of such medium limit the high-frequency scaling of practical “metamaterial” implementations based on subwavelength inclusions (e.g., split-ring resonators). Thus, for the optical range, *non-magnetic* implementations, based on approximate reductions of the constitutive parameters, have been proposed.

In this paper, we present an alternative approach to non-magnetic coordinate-transformation cloaking, based on the mapping from a *nearly-transparent*, anisotropic and spatially inhomogeneous virtual domain. We show that, unlike its counterparts in the literature, our approach is amenable to *exact analytic* treatment, and that its overall performance is comparable to that of a non-ideal (lossy, dispersive, parameter-truncated) implementation of standard (magnetic) cloaking.

PACS numbers: 41.20.Jb, 42.25.Fx, 42.25.Gy

I. INTRODUCTION AND BACKGROUND

Invisibility of objects to an interrogating (electromagnetic, acoustic, elastic, quantum) wave illumination is a fascinating research topic of long-standing interest, with a wealth of intriguing theoretical and application-oriented implications. For instance, in electromagnetics (EM) engineering, “invisible” sources, scatterers and antennas have been investigated for several decades (see, e.g., Refs. 1,2,3,4,5,6 for a sparse sampling). However, during the last few years, interest in this topic has gained renewed momentum, under the suggestive association with the “cloaking”⁷ concept, mainly motivated by the rapid advances in the engineering of “metamaterials” with precisely controllable constitutive (e.g., anisotropy, spatial inhomogeneity, dispersion) properties. Among the most prominent approaches to (passive) invisibility cloaking, it is worth recalling those based on scattering cancellation^{8,9}, coordinate transformations^{10,11,12,13} (experimentally demonstrated at microwave⁷ and visible¹⁴ frequencies), anomalous localized resonances¹⁵, inverse design of scattering optical elements¹⁶, and transmission-line networks¹⁷. The reader is referred to Ref. 18 (and references therein) for a recent comparative review of these various approaches.

In particular, the coordinate-transformation (also referred to as “transformation-optics” or “transformation EM”) approach^{10,11,12,13}, directly related to our investigation, relies on the formal invariance of Maxwell’s equations under coordinate transformations, which allows a preliminary design in an auxiliary curved-coordinate space containing a “hole,” and its subsequent translation into a conventionally flat, Cartesian space filled by an anisotropic and spatially inhomogeneous “transformation medium” that suitably bends the ray trajectories so as to re-route the energy flux around the concealment

region. The reader is referred to Refs. 19 and 20 (and references therein) for a recent collection and review of applications and theoretical aspects. Among the most interesting new twists and extensions of the basic cloaking idea above, it is worth mentioning the concepts of EM “wormhole”²¹, anti-cloak^{22,23}, carpet cloak^{24,25,26,27}, cloak at a distance²⁸, and open cloak²⁹, as well as the extensions to acoustic^{30,31}, elastic³², and quantum³³ waves.

In view of the considerable complexity of the arising transformation media, EM modeling of such structures typically relies on heavily numerical (finite-element) simulations³⁴. Nevertheless, at least for canonical (e.g., cylindrical^{35,36} and spherical³⁷) geometries, analytic full-wave approaches, based on suitable mappings of standard Fourier-Bessel or Mie expansions, have been developed. Remarkably, via these approaches, it was possible to prove analytically that in the ideal case (implying a lossless, anisotropic, spatially inhomogeneous transformation medium, with extreme values of the constitute parameters ranging from zero to infinity) the cloaking would be *perfect*, i.e., without any transmission into the concealment region and any external scattering, and may be, in principle, attained at *any* frequency – not necessarily in the asymptotic high-frequency regime that the intuitive ray-bending picture would suggest. However, the inherent limitations arising from the unavoidable losses^{35,37}, dispersion^{38,39}, perturbations³⁶ and simplifications/reductions⁴⁰ in the constitutive parameters were also pointed out.

The first experimental verification of coordinate-transformation cloaking was achieved at microwave (X-band) frequencies⁷, where the involved scales allowed the metamaterial fabrication via low-loss metallic split-ring-resonator inclusions. High-frequency scaling of this technological solution seems to be within reach for the low-THz region⁴¹, but is limited by satura-

tion effects⁴². Thus, for the visible range, an alternative route has been followed, based on the use of *non-magnetic* materials^{43,44,45}, which has led to the experimental demonstration of an optical cloak¹⁴. Non-magnetic approaches to coordinate-transformation cloaking are based on approximate reductions of the constitutive parameters that preserve the ray trajectories inside the cloak shell, at the expense of destroying the perfect impedance matching with the background medium, which can only be partially restored by suitable tweaking of the extra parameters available in quadratic^{43,44,45} or higher-order^{46,47} coordinate transformations. The above parameter reductions also prevent application of the exact analytic approaches in Refs. 35,36,37, and thus their analytic modeling is limited to asymptotic (semiclassical) approximations⁴⁸.

In this paper, we propose a different approach to non-magnetic coordinate-transformation cloaking which, acknowledging the inherent limitations of realistic metamaterial implementations, instead of applying the coordinate transformation to a *perfectly transparent* virtual domain (as in standard transformation optics), considers a *weakly non-transparent* anisotropic and spatially inhomogeneous domain. With reference to a two-dimensional (cylindrical) scenario, we show that, via a judicious choice of the constitutive parameters and the coordinate transformation, it is possible to achieve a non-magnetic transformation-medium without resorting to approximate reductions, thereby maintaining the applicability of the computationally-effective and insight-providing exact analytic modeling (via generalization of the results in Refs. 35 and 36). Moreover, via suitable parameter optimization at a given frequency, the inherently non-zero scattering can be minimized so that, when the unavoidable non-idealities (losses, dispersion, parameter truncations) of metamaterial implementations are taken into account, the overall performance becomes comparable to that of a standard (magnetic) cloak within broad parametric ranges.

Accordingly, the rest of the paper is laid out as follows. In Sec. II, we outline the problem formulation and the proposed strategy. In Sec. III, we derive the analytic solutions. In Sec. IV, we present some representative results from our parametric studies, and compare them with those achievable via standard (magnetic) cloaking. Finally, in Sec. V, we provide some concluding remarks and hints for future research.

II. PROBLEM FORMULATION AND PROPOSED STRATEGY

A. Virtual Space: Nearly-Transparent Domain

In the two-dimensional (2-D) scenario of interest, we start considering an auxiliary virtual space (x', y', z) featuring a circular cylindrical domain (infinite along z) of radius R_2 , made of an anisotropic and radially in-

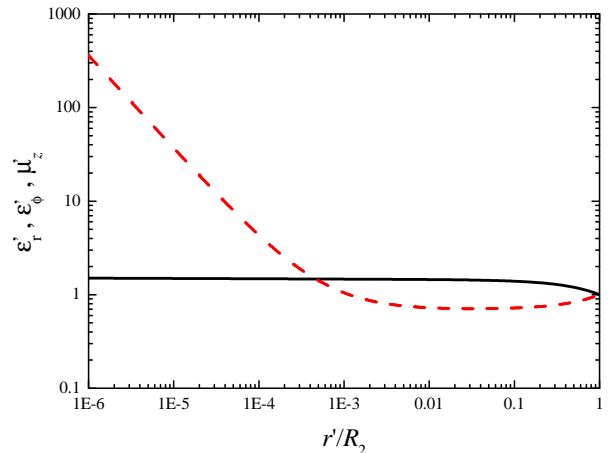


FIG. 1: (Color online) Virtual-domain-medium constitutive parameters $\varepsilon'_r = \varepsilon'_\phi$ (black solid) and μ'_z (red dashed) in (1), optimized for near-transparency at $R_2 = 3\lambda_0$ ($\gamma = 3.41 \cdot 10^{-3}$, $p = 5.41 \cdot 10^{-4}$, $\alpha = 0.361$, see Sec. IV A).

homogeneous medium immersed in vacuum. We choose for the relative permittivity and permeability tensors ($\underline{\underline{\varepsilon}}'$ and $\underline{\underline{\mu}}'$, respectively) a rather general parametric form featuring several degrees of freedom and yet amenable to analytic solution of the relevant Helmholtz equation; for the transverse-magnetic (TM) polarization (magnetic field parallel to the cylinder) of interest here, their relevant components (in the associated cylindrical coordinates r', ϕ, z) are given by

$$\varepsilon'_r(r') = \varepsilon'_\phi(r') = \left(\frac{r'}{R_2}\right)^{-\gamma} \exp\left[-\alpha\left(\frac{r'}{R_2} - 1\right)\right], \quad (1a)$$

$$\mu'_z(r') = P(r') \left(\frac{r'}{R_2}\right)^\gamma \exp\left[\alpha\left(\frac{r'}{R_2} - 1\right)\right], \quad (1b)$$

where $\gamma > 0$, $\alpha > 0$, and

$$P(r') = 1 - p + p\frac{R_2}{r'}, \quad 0 \leq p \leq 1. \quad (2)$$

Note that the constitutive parameters in (1) are always positive, and locally matched with vacuum at the interface $r' = R_2$, whereas they may exhibit singular behaviors at $r' = 0$,

$$\lim_{r' \rightarrow 0} \varepsilon'_{r,\phi}(r') = \infty, \quad \lim_{r' \rightarrow 0} \mu'_z(r') = \begin{cases} \infty, & 0 < \gamma < 1, \\ \exp(-\alpha)p, & \gamma = 1, \\ 0, & \gamma > 1. \end{cases} \quad (3)$$

We highlight that, unlike the typical transformation-optics framework, our virtual domain is *not* perfectly transparent. Nevertheless, the constitutive relationships in (1) contain three adjustable parameters (α, γ, p) that can be optimized (see Sec. IV A below) for achieving a *nearly-transparent* response at a given frequency. Figure

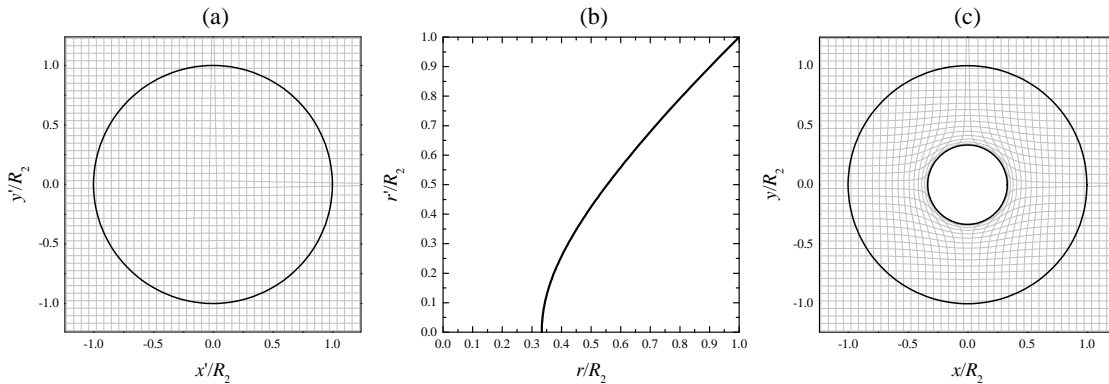


FIG. 2: (a) Ray trajectories (thin grey curves, traced along the positive x' and y' directions) in the virtual domain, with parameters as in Fig. 1. (b) Coordinate transformation $r = g(r')$ vs. $r' = f(r)$ [cf. (9)–(11)] for $R_1 = R_2/3$. (c) Ray trajectories in the transformed domain. The black thick circles delimit the $r = R_1$ and $r = R_2$ cylindrical domains.

1 shows an example of constitutive parameters optimized for an electrical size $R_2 = 3\lambda_0$ (with λ_0 denoting the vacuum wavelength). The log-log scale utilized highlights the algebraic singular behavior of the permeability for $r' \rightarrow 0$, but is still not able to capture the extremely slow (in view of the chosen parameters) divergence of the permittivities. For the same configuration, Fig. 2(a) illustrates the ray tracing, obtained as in Ref. 13. As a first indication of the nearly-transparent behavior of this optimized parametric configuration, one can observe the *practically straight* ray trajectories, with only a slight bending for those passing nearby the cylinder center.

B. Coordinate Transformation

Following the transformation-optics approach^{10,11,12,13}, in order to achieve invisibility cloaking, we construct a cylindrical coordinate transformation, from the virtual space (x', y', z) to the actual physical space (x, y, z) of interest,

$$r = g(r'), \quad r' \leq R_2, \quad (4)$$

which compresses the cylindrical nearly-transparent region $r' \leq R_2$ into a concentric annulus $R_1 \leq r \leq R_2$, i.e., satisfies the boundary conditions

$$g(0) = R_1, \quad g(R_2) = R_2. \quad (5)$$

As previously mentioned, the non-flat metric underlying the transformation in (4) and (5) creates a “hole” of radius R_1 , i.e., a region of space *effectively impenetrable* by the EM fields where an object can be concealed. Invoking the formal invariance of Maxwell’s equations under coordinate transformations, the above behavior can be equivalently obtained in a *globally flat* space by filling up the transformed region $R_1 \leq r \leq R_2$ with an anisotropic, spatially inhomogeneous “transformation

medium,” whose relative permittivity and permeability tensors ($\underline{\underline{\varepsilon}}$ and $\underline{\underline{\mu}}$, respectively) are given by^{10,11,12,13}

$$\left\{ \begin{array}{c} \underline{\underline{\varepsilon}} \\ \underline{\underline{\mu}} \end{array} \right\} = \underline{\underline{J}} \cdot \left\{ \begin{array}{c} \underline{\underline{\varepsilon'}} \\ \underline{\underline{\mu'}} \end{array} \right\} \cdot \underline{\underline{J}}^T [\det(\underline{\underline{J}})]^{-1}, \quad (6)$$

where $\underline{\underline{J}} = \partial(x, y, z)/\partial(x', y', z)$ is the Jacobian matrix of the transformation in (4), the superfix T indicates transposition, and the symbol $\det(\cdot)$ denotes the determinant. For the TM polarization of interest here, the relevant (cylindrical) components can be directly found from (1) as⁴³

$$\varepsilon_r(r) = \varepsilon'_r(r') \dot{g}(r') \frac{r'}{r}, \quad (7a)$$

$$\varepsilon_\phi(r) = \frac{\varepsilon'_\phi(r')}{\dot{g}(r')} \frac{r}{r'}, \quad (7b)$$

$$\mu_z(r) = \frac{\mu'_z(r')}{\dot{g}(r')} \frac{r'}{r}, \quad (7c)$$

where the overdot $\dot{\cdot}$ denotes differentiation with respect to the argument, and $r' = f(r)$ [with $f(r) \equiv g^{-1}(r')$ denoting the inverse mapping]. In standard approaches to *non-magnetic* cloaking^{43,44,45,46,47}, based on perfectly-transparent virtual domains (i.e., $\varepsilon'_r = \varepsilon'_\phi = \mu'_z = 1$), reliance is made on the dependence of the ray trajectories on the products $\varepsilon_r \mu_z$ and $\varepsilon_\phi \mu_z$ in order to find a set of reduced parameters featuring $\mu_z = 1$. As anticipated, this destroys the perfect transparency of the cloak, and prevents application of the exact analytic framework in Refs. 35 and 36. In our approach, instead, we capitalize on the extra degrees of freedom available in order to enforce $\mu_z(r) = 1$ in (7c), which yields the following first-order differential equation

$$\dot{g}(r') - \frac{r' \mu'_z(r')}{g(r')} = 0. \quad (8)$$

A similar approach was used in Ref. 49 in order to obtain a spatially homogeneous axial permeability (or permit-

tivity, for the transverse-electric polarization). However, relying on a vacuum (i.e., $\varepsilon' = \mu' = 1$) virtual domain, such approach did not provide enough degrees of freedom. As a consequence, once the cloaking boundary conditions in (5) were enforced, the value of the transformed axial permeability was inevitably dictated by the shape factor R_1/R_2 , and (most important) *always larger* than the vacuum value (i.e., $\mu_z > 1$, for the case of interest here). In our approach, this limitation is overcome via the extra degrees of freedom endowed by the virtual-domain permeability $\mu'_z(r')$ [cf. Eqs. (1b) and (2)]. In particular, thanks to the functional form in (1b), the differential equation in (8) admits a closed-form analytic solution as

$$g(r') = \sqrt{R_1^2 + R_2^2 h\left(\frac{r'}{R_2}; \alpha, \gamma, p\right)}, \quad (9)$$

where

$$h\left(\frac{r'}{R_2}; \alpha, \gamma, p\right) = 2 \exp(-\alpha) \times \left[\left(\frac{1-p}{\gamma+2}\right) \left(\frac{r'}{R_2}\right)^{\gamma+2} M\left(\gamma+2, \gamma+3, \frac{\alpha r'}{R_2}\right) + \left(\frac{p}{\gamma+1}\right) \left(\frac{r'}{R_2}\right)^{\gamma+1} M\left(\gamma+1, \gamma+2, \frac{\alpha r'}{R_2}\right) \right], \quad (10)$$

with $M(\cdot, \cdot, \cdot)$ denoting the confluent hypergeometric function [Eq. (13.1.2) in Ref. 50]. Note that, in light of the assumed constraints ($\alpha > 0$, $\gamma > 0$, $0 \leq p \leq 1$), the function $h(r'/R_2; \alpha, \gamma, p)$ in (10) is always positive, which ensures that the mapping $g(r')$ in (9) is always real. Moreover, in (9) and (10), the arising integration constant has been exploited to enforce the first boundary condition in (5); the second boundary condition, instead, yields

$$h(1; \alpha, \gamma, p) = 1 - \left(\frac{R_1}{R_2}\right)^2, \quad (11)$$

which can be satisfied by properly tweaking the parameters α , γ , and p . In particular, in view of the *linear* dependence involved, Eq. (11) may be straightforwardly solved with respect to p . However, this seemingly simplest approach is not necessarily the most effective in a broader perspective of achieving a nearly-transparent response. In fact, our parametric studies (see Sec. IV A below) indicate that it is generally more convenient to satisfy the constraint in (11) by fixing α (via numerical solution), and exploit the parameters γ and p for minimizing the scattering response.

It should be noted that, since $\mu'_z(r')$ in (1b) and $g(r')$ in (9) are always positive, the constraint in (8) also implies $\dot{g}(r') > 0$, and hence the invertibility of the coordinate mapping. However, the inverse mapping $f(r) = g^{-1}(r')$ cannot generally be calculated analytically. Nevertheless, as can be observed from the example in Fig. 2(b), the mapping behavior is fairly regular, and therefore its

numerical inversion does not pose any problem. Figure 2(c) shows the ray trajectories obtained by transforming [via the mapping in Fig. 2(b)] those in the virtual space [cf. Fig. 2(a)], from which the ray bending around the interior region ($r < R_1$) to conceal (typical of coordinate-transformation-based cloaking) is fairly evident.

C. Real Space: Non-Magnetic Transformation Medium

By substituting (1) and $r' = f(r)$ in (7), and taking into account (8), we readily obtain the explicit expressions of the constitutive parameters of the desired *non-magnetic* transformation medium in the real space,

$$\varepsilon_r(r) = \frac{R_2^\gamma [f(r)]^{1-\gamma}}{r \dot{f}(r)} \exp\left\{-\alpha \left[\frac{f(r)}{R_2} - 1\right]\right\}, \quad (12a)$$

$$\varepsilon_\phi(r) = \frac{R_2^\gamma r \dot{f}(r)}{[f(r)]^{\gamma+1}} \exp\left\{-\alpha \left[\frac{f(r)}{R_2} - 1\right]\right\}, \quad (12b)$$

$$\mu_z(r) = 1. \quad (12c)$$

Note that, since $f(r)$ and $\dot{f}(r)$ are always positive in the transformed region $R_1 \leq r \leq R_2$, both permittivity components in (12a) and (12b) are likewise positive, thereby yielding a *double positive* medium. Moreover, like the virtual-space medium in (1), our non-magnetic transformation medium in (12) is locally matched with vacuum at $r = R_2$. In view of the singular behavior exhibited by the virtual-domain medium at $r' = 0$ [cf. (3)], it is interesting to investigate the behavior of the transformation medium at the image point $r = R_1$. Recalling that $M(a, b, 0) = 1$ [cf. Eq. (13.1.2) in Ref. 50], we obtain from (10), in the limit $r' \rightarrow 0$,

$$h\left(\frac{r'}{R_2}; \alpha, \gamma, p\right) \sim 2 \exp(-\alpha) \left(\frac{\chi}{\gamma - s + 2}\right) \left(\frac{r'}{R_2}\right)^{\gamma-s+2}, \quad (13)$$

where

$$\chi = \begin{cases} 1, & p = 0, \\ p, & p \neq 0, \end{cases} \quad s = \begin{cases} 0, & p = 0, \\ 1, & p \neq 0. \end{cases} \quad (14)$$

By substituting (13) into (9), and approximating the square root via its first-order Taylor expansion, we then obtain

$$g(r') \sim R_1 \sqrt{1 + \frac{2 \exp(-\alpha) \chi R_2^{s-\gamma} (r')^{\gamma-s+2}}{(\gamma-s+2) R_1^2}} \sim R_1 + \frac{\exp(-\alpha) \chi R_2^{s-\gamma} (r')^{\gamma-s+2}}{(\gamma-s+2) R_1}, \quad (15a)$$

and hence, via differentiation,

$$\dot{g}(r') \sim \exp(-\alpha) \chi R_1^{-1} R_2^{s-\gamma} (r')^{\gamma-s+1}. \quad (15b)$$

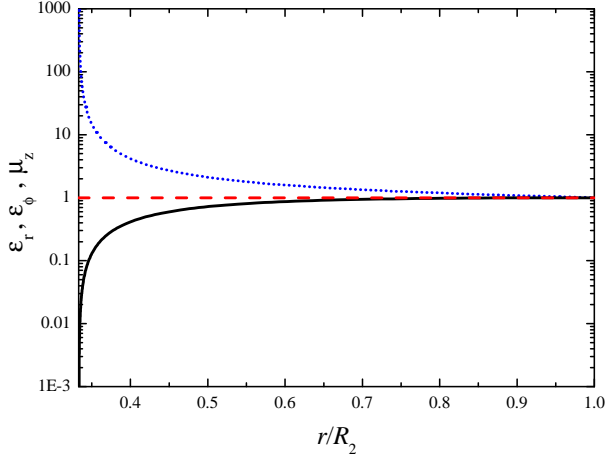


FIG. 3: (Color online) Non-magnetic transformation-medium constitutive parameters ε_r (black solid), ε_ϕ (blue dotted) and μ_z (red dashed) in (12), obtained from the nearly-transparent virtual domain in Fig. 1 via the mapping in Fig. 2(b).

Recalling that $\dot{f}(r) = 1/\dot{g}(r')$ and $r' = f(r)$, and substituting into (12a) and (12b), we then obtain

$$\varepsilon_r(r) \sim \frac{\chi R_2^s}{R_1^2} [f(r)]^{2-s}, \quad (16a)$$

$$\varepsilon_\phi(r) \sim \frac{\exp(2\alpha) R_1^2 R_2^{2\gamma-s}}{\chi} [f(r)]^{s-2\gamma-2}, \quad (16b)$$

from which, recalling that $0 \leq s \leq 1$ and $\gamma > 0$, it finally follows

$$\varepsilon_r(R_1) = 0, \quad \lim_{r \rightarrow R_1} \varepsilon_\phi(r) = \infty. \quad (17)$$

Thus, as in standard (magnetic) cloaking, at the inner interface $r = R_1$, the permittivities exhibit either zero or infinite values. Figure 3 shows the transformation-medium constitutive parameters obtained from the (optimized) virtual-domain medium in Fig. 1, via the coordinate mapping in Fig. 2(b), and corresponding to the ray trajectories in Fig. 2(c).

It is worth pointing out that, in principle, different choices of the parameters and functional forms of the virtual-domain medium (1) are possible, yielding *finite* variation ranges of the resulting transformation media. Our choice here was only aimed at facilitating direct comparison with standard (magnetic) cloaks. Nevertheless, the effects of unavoidable parameter truncations are investigated in our parametric studies (see Sec. IV B below).

III. ANALYTIC SOLUTIONS

The EM response of the cloaking configuration of interest can be computed analytically by generalizing the

Fourier-Bessel-type approach in Refs. 35 and 36. In what follows, we address such generalization for the case of TM-polarized plane-wave illumination with unit-amplitude z -directed magnetic field and time-harmonic $[\exp(-i\omega t)]$ dependence, by suitable coordinate mapping [via the inverse of (4)] of the virtual-space solution.

A. Virtual Space

It is expedient to expand the incident plane wave H_z^i (assumed to impinge from the positive x' direction) and the scattered field H_z^s into Fourier-Bessel series,

$$\begin{aligned} H_z^i(r', \phi) &= \exp(ik_0 x') \\ &= \sum_{m=-\infty}^{\infty} i^m J_m(k_0 r') \exp(im\phi), \end{aligned} \quad (18a)$$

$$H_z^s(r', \phi) = \sum_{m=-\infty}^{\infty} c_m H_m^{(1)}(k_0 r') \exp(im\phi), \quad (18b)$$

where $k_0 = \omega/c = 2\pi/\lambda_0$ denotes the vacuum wavenumber (with c denoting the speed of light in vacuum), $J_m(\cdot)$ and $H_m^{(1)}(\cdot)$ are the m -th order Bessel and Hankel functions of first kind, respectively (cf. Sec. 9.1 in Ref. 50), and c_m are unknown coefficients. The magnetic field H_z^t transmitted inside the cylindrical domain $r' < R_2$, ruled by the Helmholtz equation³⁵

$$\begin{aligned} \frac{1}{r' \mu_z'(r')} \frac{\partial}{\partial r'} \left[\frac{r'}{\varepsilon_\phi'(r')} \frac{\partial}{\partial r'} \right] H_z^t(r', \phi) \\ + \left[\frac{1}{r'^2 \varepsilon_r'(r') \mu_z'(r')} \frac{\partial^2}{\partial \phi^2} + k_0^2 \right] H_z^t(r', \phi) = 0, \end{aligned} \quad (19)$$

can be likewise expanded into this type of series

$$\begin{aligned} H_z^t(r', \phi) &= \sum_{m=-\infty}^{\infty} \left[a_m \Psi_m^{(1)}(k_0 r') + b_m \Psi_m^{(2)}(k_0 r') \right] \\ &\times \exp(im\phi), \quad r' \leq R_2. \end{aligned} \quad (20)$$

In (20), a_m and b_m are unknown coefficients, while $\Psi_m^{(1,2)}(\cdot)$ denote independent solutions of the radial Helmholtz equations

$$\begin{aligned} \left\{ \frac{d^2}{dr'^2} + \left[\frac{1}{r'} - \frac{1}{\varepsilon_\phi'(r')} \frac{d\varepsilon_\phi'(r')}{dr'} \right] \frac{d}{dr'} \right\} \Psi_m(k_0 r') \\ + \left[k_0^2 \mu_z'(r') \varepsilon_\phi'(r') - \frac{m^2 \varepsilon_\phi'(r')}{r'^2 \varepsilon_r'(r')} \right] \Psi_m(k_0 r') = 0. \end{aligned} \quad (21)$$

It can be shown (see Appendix A for details) that, for the constitutive parameters in (1), these solutions can be expressed in closed form as

$$\begin{aligned} \Psi_m^{(1,2)}(k_0 r') &= \left(\frac{r'}{R_2} \right)^{\frac{\nu_m - \gamma}{2}} \exp \left[-\frac{(\alpha + \xi R_2) r'}{2R_2} \right] \\ &\times \left\{ \begin{array}{l} M(\zeta_m, \nu_m + 1, \xi r') \\ U(\zeta_m, \nu_m + 1, \xi r') \end{array} \right\}, \end{aligned} \quad (22)$$

where (the already defined) $M(\cdot, \cdot, \cdot)$ and $U(\cdot, \cdot, \cdot)$ are confluent hypergeometric functions [cf. Eqs. (13.1.2) and (13.1.3), respectively, in Ref. 50], and

$$\nu_m = \sqrt{\gamma^2 + 4m^2}, \quad (23a)$$

$$\xi = R_2^{-1} \sqrt{\alpha^2 - 4(1-p)k_0^2 R_2^2}, \quad 0 \leq \arg(\xi) < \pi, \quad (23b)$$

$$\zeta_m = \frac{\xi(\nu_m + 1)R_2 + \alpha(\gamma + 1) - 2pk_0^2 R_2^2}{2\xi R_2}. \quad (23c)$$

Recalling that the wavefunctions $\Psi_m^{(2)}$ exhibit a singular behavior at $r' = 0$ (see Appendix B), the field-finiteness condition yields $b_m = 0$ in (20). The remaining unknown expansion coefficients (a_m and c_m) can be computed by enforcing the continuity of the magnetic and electric field tangential components at the interface $r = R_2$, viz.,

$$H_z^t(R_2, \phi) = H_z^i(R_2, \phi) + H_z^s(R_2, \phi), \quad (24a)$$

$$E_\phi^t(R_2, \phi) = E_\phi^i(R_2, \phi) + E_\phi^s(R_2, \phi), \quad (24b)$$

where the tangential electric fields readily follow from the curl Maxwell equation

$$E_\phi(r', \phi) = \frac{1}{i\omega\epsilon_0\epsilon'_\phi(r')} \frac{\partial H_z(r', \phi)}{\partial r'}. \quad (25)$$

By substituting the Fourier expansions (18) and (20) into (24) [with (25)], we obtain a doubly countable infinity of linear equations,

$$a_m \Psi_m^{(1)}(k_0 R_2) = i^m J_m(k_0 R_2) + c_m H_m^{(1)}(k_0 R_2), \quad (26a)$$

$$a_m \dot{\Psi}_m^{(1)}(k_0 R_2) = i^m \dot{J}_m(k_0 R_2) + c_m \dot{H}_m^{(1)}(k_0 R_2), \quad (26b)$$

which can be solved in a straightforward fashion, yielding

$$a_m = \frac{2i^{m+1}}{\pi k_0 R_2 W_{[H_m^{(1)}, \Psi_m^{(1)}]}}, \quad (27a)$$

$$c_m = \frac{-i^m W_{[J_m, \Psi_m^{(1)}]}}{W_{[H_m^{(1)}, \Psi_m^{(1)}]}}, \quad (27b)$$

where $W_{[F,G]}$ represents the Wronskian of the functions F and G evaluated at $k_0 R_2$,

$$W_{[F,G]} = F(k_0 R_2) \dot{G}(k_0 R_2) - \dot{F}(k_0 R_2) G(k_0 R_2). \quad (28)$$

B. Real Space

We can now address the solution in the real space (r, ϕ, z) , by generalizing the approach in Refs. 35 and 36. First, we note that, since the coordinate transformation in (4) is restricted within the cloak shell $R_1 \leq r \leq R_2$, the fields in the (vacuum) exterior region $r > R_2$ admit the same expressions as in (18) (with r substituting r'). For the same reason, the field transmitted into the (vacuum) concealment region $r \leq R_1$, can be expanded in terms of a standard Fourier-Bessel series,

$$H_z^t(r, \phi) = \sum_{m=-\infty}^{\infty} d_m J_m(k_0 r) \exp(im\phi), \quad r \leq R_1, \quad (29a)$$

where d_m are unknown coefficients, and the field-finiteness condition has been enforced. Following Refs. 35 and 36, the field transmitted into the cloak shell $R_1 \leq r \leq R_2$ is obtained by (inverse) coordinate mapping [via (4)] of the virtual-space solution (20), viz.,

$$H_z^t(r, \phi) = \sum_{m=-\infty}^{\infty} \left[a_m \psi_m^{(1)}(k_0 r) + b_m \psi_m^{(2)}(k_0 r) \right] \times \exp(im\phi), \quad R_1 \leq r \leq R_2, \quad (29b)$$

where a_m and b_m are unknown expansion coefficients, and

$$\psi_m^{(1,2)}(k_0 r) = \Psi_m^{(1,2)}[k_0 f(r)]. \quad (30)$$

Once again, the four sets of unknown expansion coefficients (a_m, b_m, c_m, d_m) can be computed by enforcing the continuity of the tangential fields, this time at the interfaces $r = R_1$ and $r = R_2$. While the continuity at the outer interface ($r = R_2$) does not pose any particular problem, much more involved is dealing with the inner interface ($r = R_1$), in view of the singular behavior exhibited by the wavefunctions $\psi_m^{(2)}$ in (30) [cf. Eq. (13.1.3) in Ref. 50, and Appendix B] and the azimuthal permittivity ϵ_ϕ in (12b) [cf. (17)]. In order to circumvent this problem, as in Refs. 35 and 36, we therefore follow a limiting approach, slightly shifting the inner cloak boundary to $r = R_1 + \Delta$, where Δ denotes a small quantity (which eventually we let tend to zero). Accordingly, we obtain

$$d_m J_m[k_0(R_1 + \Delta)] = a_m \psi_m^{(1)}[k_0(R_1 + \Delta)] + b_m \psi_m^{(2)}[k_0(R_1 + \Delta)], \quad (31a)$$

$$d_m \dot{J}_m[k_0(R_1 + \Delta)] = \frac{a_m \dot{\psi}_m^{(1)}[k_0(R_1 + \Delta)] + b_m \dot{\psi}_m^{(2)}[k_0(R_1 + \Delta)]}{\epsilon_\phi(R_1 + \Delta)}, \quad (31b)$$

$$a_m \psi_m^{(1)}(k_0 R_2) + b_m \psi_m^{(2)}(k_0 R_2) = i^m J_m(k_0 R_2) + c_m H_m^{(1)}(k_0 R_2), \quad (31c)$$

$$a_m \dot{\psi}_m^{(1)}(k_0 R_2) + b_m \dot{\psi}_m^{(2)}(k_0 R_2) = i^m \dot{J}_m(k_0 R_2) + c_m \dot{H}_m^{(1)}(k_0 R_2). \quad (31d)$$

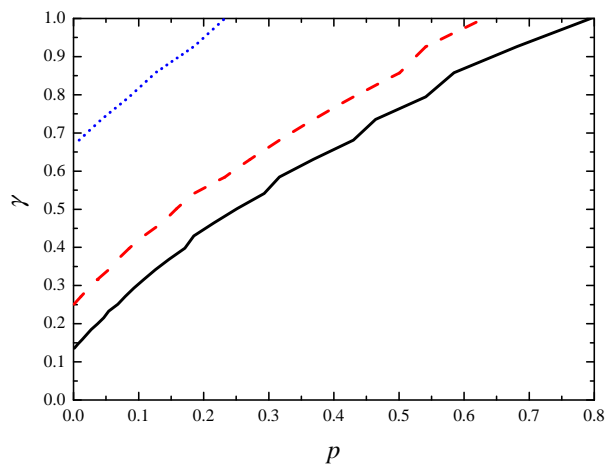


FIG. 4: (Color online) Curves in the (γ, p) plane yielding $\alpha = 0$ roots of (11), for the parameters in Fig. 1 and shape-factor values $R_1/R_2 = 1/4, 1/3, 1/2$ (black-solid, red-dashed, blue-dotted, respectively). The regions below the curves are associated with positive α values, and thus represent the admissible (γ, p) search spaces in the scattering-width minimization problem.

It can be shown (see Appendix B for details) that, in the limit $\Delta \rightarrow 0$, Eqs. (31a) and (31b) yield

$$b_m \sim a_m \Omega_1 \left(\frac{\Delta}{R_2} \right)^{\frac{\nu_m}{\gamma-s+2}}, \quad (32a)$$

$$d_m \sim a_m \Omega_2 \left(\frac{\Delta}{R_2} \right)^{\frac{\gamma+\nu_m}{2(\gamma-s+2)}}, \quad (32b)$$

where $\Omega_{1,2}$ are irrelevant constants. Recalling that $0 \leq s \leq 1$, $\gamma > 0$ and $\nu_m > 0$, it is readily realized that the expansion coefficients b_m and d_m in (32) vanish as $\Delta \rightarrow 0$. As a consequence, recalling (30) and that $f(R_2) = R_2$, Eqs. (31c) and (31d) are readily recognized to become identical to (26a) and (26b), respectively, and therefore the remaining unknown coefficients a_m and c_m are still given by (27).

To sum up, the above analytic solutions resemble those obtained for the standard (magnetic) cloak³⁵ in the *exact suppression* of the field transmitted into the concealment region (i.e., $d_m = 0$). The expectable differences show up in the *non-zero* scattering coefficients c_m , which are directly inherited from the nearly-transparent medium (1) in the virtual space.

In what follows, we show that, via judicious optimization at a given frequency, the scattering response can be effectively reduced so that the overall performance of the proposed nonmagnetic cloak becomes comparable to that of a standard (magnetic) cloak when the unavoidable non-idealities (parameter truncations, losses, dispersion) are taken into account.

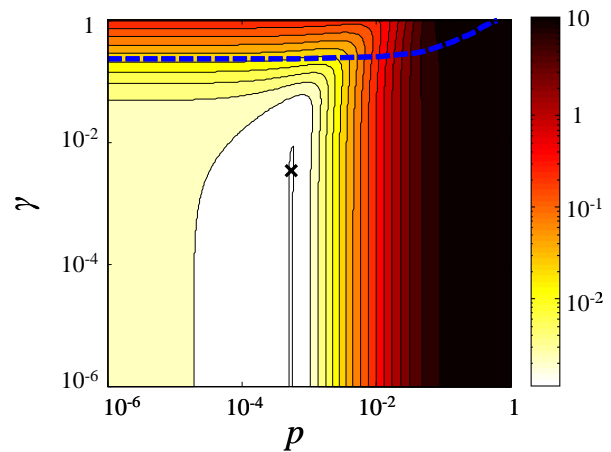


FIG. 5: (Color online) Contour plot of the scattering width in (33) as a function of γ and p , for the parameters in Fig. 1 and shape factor $R_1/R_2 = 1/3$. The blue-dashed curve delimits the admissible search space (cf. Fig. 4), whereas the cross indicates the minimum.

IV. REPRESENTATIVE RESULTS

We now move on to the presentation of the salient results from an extensive series of parametric studies, starting with the virtual-domain parameter optimization, and continuing with the performance comparison between the proposed approach and standard (magnetic) cloaking.

A. Virtual Space: Optimization for Near-Transparency

As previously mentioned, the inherently non-zero scattering response of our proposed non-magnetic cloak is directly inherited by the non-transparent virtual domain in (1). In our study, such response is compactly parameterized in terms of the total scattering cross-sectional width per unit length⁹

$$Q_s = \frac{4}{k_0} \sum_{m=-\infty}^{\infty} |c_m|^2, \quad (33)$$

where the scattering coefficients c_m are given by (27b). Our approach is based on the minimization of the scattering width in (33), at a given frequency, by acting on the free parameters (α, γ, p) available in the virtual-domain-medium constitutive parameters (1). Clearly, different observables (e.g., more directly tied to the near-field or angular distributions) may be considered, giving rise to different optimized configurations. It is also worth recalling that the above parameters are actually constrained via the cloak condition in (11). In our numerical studies, we found it most effective to satisfy this constraint by fixing α via numerical solution of (11), and exploit the parameters γ and p for minimizing Q_s . Figure 4 shows,

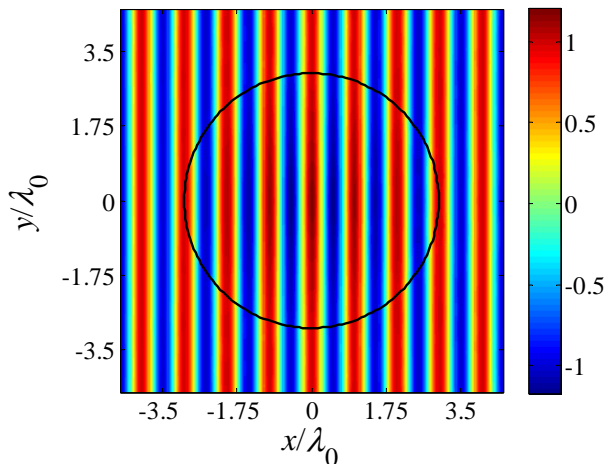


FIG. 6: (Color online) Magnetic field (real part) map in the virtual space, for unit-amplitude TM-polarized plane-wave illumination (impinging along the positive x -direction), and with ideal (lossless, non-truncated) parameters as in Fig. 1.

for representative values of the shape factor R_1/R_2 , the (γ, p) parametric ranges for which (11) admits a solution $\alpha > 0$ (consistent with the model assumptions), which constitute the search spaces in our minimization problem⁵¹. In view of the reduced number of parameters involved and the computationally-effective analytic modeling, such minimization can be readily pursued via exhaustive parameter scanning. For a fixed frequency and shape factor, Fig. 5 shows the scattering width in (33) as a function of the two free parameters γ and p , within the above defined admissible ranges, from which a rather broad minimum is identified. The corresponding parameter configuration yields the constitutive relationships shown in Fig. 1 and the associated (practically straight) ray trajectories in Fig. 2(a). For the same ideal (lossless, non-truncated) parameter configuration, Fig. 6 shows the real part of the magnetic field map (for plane-wave excitation) computed via the expansions in (18) and (20) [with (27)], from which the near-transparency is evident.

B. Real Space: Comparison with Standard (Magnetic) Cloak

Referring to the non-magnetic ideal (lossless, non-truncated) constitutive parameters in Fig. 3 and associated ray trajectories in Fig. 2(c) [derived from the above optimized virtual-domain via the mapping in Fig. 2(b)], Fig. 7 shows the corresponding field map, computed via the expansions in (18) and (29) [with (27) and (32)], which highlights the cloaking effect accompanied by a *very weak* scattering (identical to that in Fig. 6).

Although the present prototype study was not focused on practical applications, we did explore the effects of the

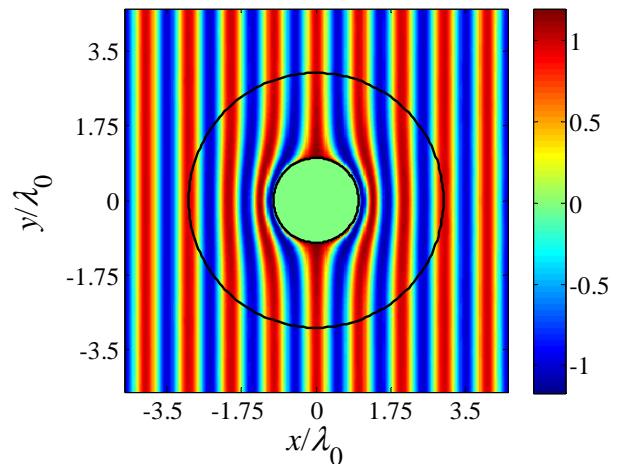


FIG. 7: (Color online) As in Fig. 6, but for the real domain, with ideal (lossless, non-truncated) parameters as in Fig. 3.

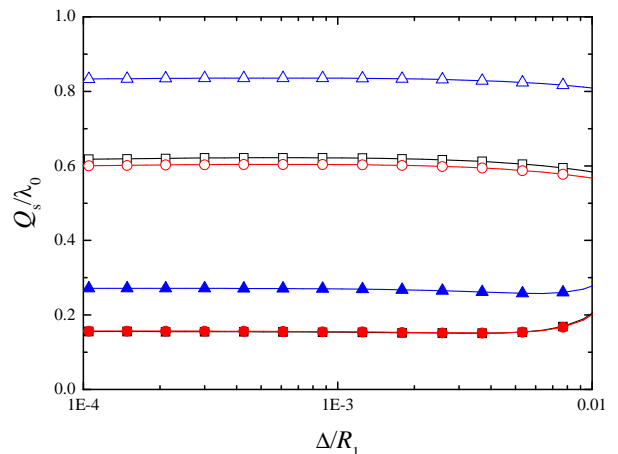


FIG. 8: (Color online) Parameters as in Fig. 3, but truncated at $r = R_1 + \Delta$. Total scattering width (normalized with respect to the vacuum wavelength), as a function of the truncation parameter Δ/R_1 , for loss-tangent values $\tan \delta = 0, 10^{-3}, 10^{-2}$ (full black squares, red circles, and blue triangles, respectively). As a reference, the corresponding values attainable from a standard (magnetic) cloak [cf. (34)] with comparable parameter truncations are displayed as empty markers.

unavoidable non-idealities, namely, the parameter truncations and material losses. As for the standard (magnetic) cloak, suitable truncation of the permittivities in (12) at the inner interface $r = R_1$ is necessary in view of their singular behavior [cf. (17)]. As in Refs. 35 and 36, in our parametric studies, we truncated the cloak shell at an interface $r = R_1 + \Delta$, considering the thin annulus $R_1 \leq r < R_1 + \Delta$ as part of the concealment region. Figure 8 shows, for an empty (vacuum) concealment region, the scattering width as a function of the truncation parameter Δ/R_1 , for various values of the loss-tangent

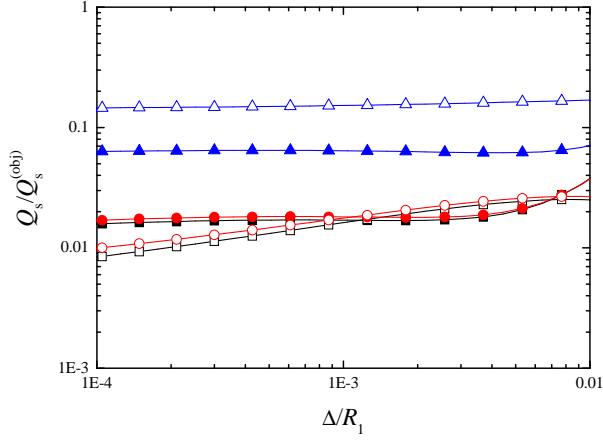


FIG. 9: (Color online) As in Fig. 8, but with the concealment region entirely filled by a dielectric object with relative permittivity $\varepsilon_{obj} = 4$. In order to better visualize the cloaking effect, the scattering width is normalized with respect to reference value $Q_s^{(obj)}$ exhibited by the object in vacuum.

ranging from zero to 10^{-2} . For comparison, we also studied the response of a standard (magnetic) cloak⁷,

$$\varepsilon_r^{(ref)}(r) = \frac{r - R_1}{r}, \quad (34a)$$

$$\varepsilon_\phi^{(ref)}(r) = \frac{r}{r - R_1}, \quad (34b)$$

$$\mu_z^{(ref)}(r) = \left(\frac{R_2}{R_2 - R_1} \right)^2 \frac{r}{r - R_1}, \quad (34c)$$

likewise truncated so as to guarantee comparable variation ranges of the permittivities⁵². As one can observe, in spite of its non-magnetic character, the proposed cloak turns out to outperform the standard one (in terms of smaller scattering width) over a wide parametric range extending up to moderate values of the truncation parameter and losses.

It is worth pointing out that parameter truncations allow field penetration through the cloak shell, and thus, unlike in the ideal case, the overall response generally depends on the possible presence of objects in the concealment region. We therefore studied some representative scenarios, with the concealment region entirely filled up by a dielectric (with relative permittivity $\varepsilon_{obj} = 4$ and 16) or a perfect electric conductor (PEC), still amenable to analytic solution via straightforward generalization of (29). Figures 9–11 show the corresponding responses, where, in order to better visualize the cloaking effect, the scattering width has been normalized with respect to the reference value $Q_s^{(obj)}$ exhibited by the object in vacuum. For all cases, it can be observed that the performance of proposed non-magnetic cloak is comparable to that of the standard cloak over wide parametric ranges. The sensible differences that may exist in certain parametric configurations (e.g., the PEC case in Fig. 11 for very small

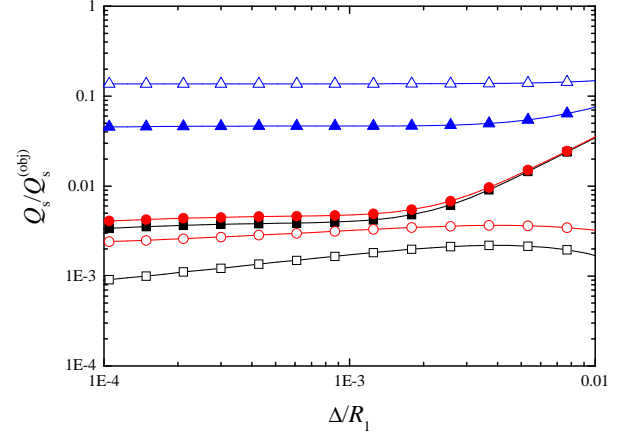


FIG. 10: (Color online) As in Fig. 9, but for an object with $\varepsilon_{obj} = 16$.

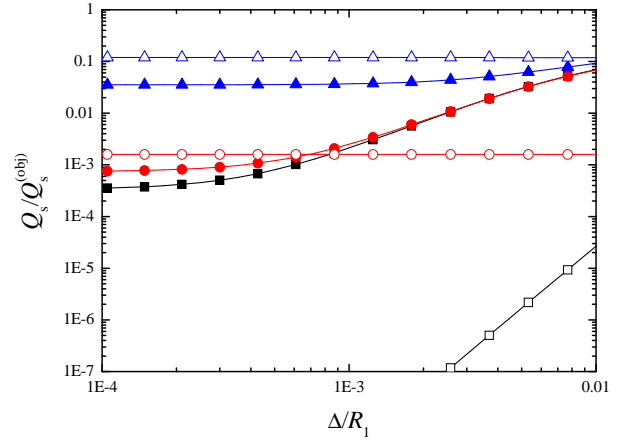


FIG. 11: (Color online) As in Fig. 9, but for a PEC object.

values of the truncation parameter Δ/R_1 and no losses) tend to disappear when moderate values of the truncation parameter and loss-tangent are considered. In particular, for $\tan \delta = 10^{-2}$, the proposed non-magnetic cloak is still capable of reducing the scattering width of over an order of magnitude with respect to the uncloaked case, slightly outperforming a comparably-truncated standard cloak. As an example, Fig. 12 compares the responses pertaining to a PEC cylinder free-standing in vacuum and cloaked with the proposed and standard approaches, for a truncation parameter $\Delta/R_1 = 10^{-2}$ and loss tangent $\tan \delta = 10^{-2}$, in terms of the bistatic scattering width

$$\begin{aligned} \sigma_s(\phi) &= \lim_{r \rightarrow \infty} 2\pi r \frac{|H_z^s(r, \phi)|^2}{|H_z^i(r, \phi)|^2} \\ &= \frac{4}{k_0} \left| \sum_{m=-\infty}^{\infty} (-i)^m c_m \exp(im\phi) \right|^2, \quad (35) \end{aligned}$$

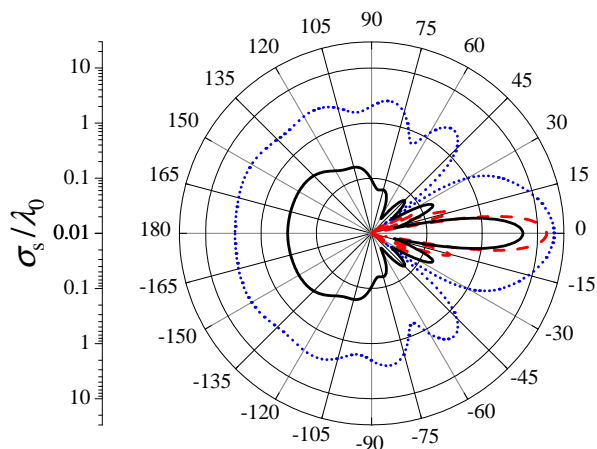


FIG. 12: (Color online) Bistatic scattering width in (35) (normalized with respect to the vacuum wavelength), for a concealment domain filled by a PEC object. Object cloaked via the proposed (black-solid; $Q_s/\lambda_0 = 0.32$) and standard (red-dashed; $Q_s/\lambda_0 = 0.41$) approach, respectively, with truncation parameter $\Delta/R_1 = 10^{-2}$ and loss-tangent $\tan \delta = 10^{-2}$. Also shown, as a reference, is the response pertaining to the object free-standing in vacuum (blue-dotted; $Q_s^{(obj)}/\lambda_0 = 3.46$).

which describes the angular distribution of the total scattering width in (33). While the total scattering width values for the proposed and standard cloaks turn out to be comparable ($Q_s/\lambda_0 = 0.32$ and 0.41 , respectively, with a reduction of about an order of magnitude as compared to the uncloaked case), certain differences are evident in the angular distributions. In particular, as compared to the uncloaked case, our proposed cloak attains a rather uniform reduction (of almost an order of magnitude, in the worst case), whereas the standard cloak seems to work much better for backscattering ($\phi = 180^\circ$) but rather poorly in the forward ($\phi = 0$) direction.

Similar results, not shown here for brevity, were obtained for different frequencies and shape factors R_1/R_2 .

To sum up, when the unavoidable parameter-truncation and loss effects are taken into account, the overall performance of our proposed strategy turns out to be comparable to that of a standard (magnetic) cloak. Moreover, it should be mentioned that the theoretically frequency-independent behavior of this latter is severely restricted by the unavoidable dispersion effects in any practical metamaterial implementation, so that the inherently *narrow-band* character of our proposed design (optimized to work at a given frequency) does not seem to constitute a critical limitation.

V. CONCLUSIONS AND OUTLOOK

In this paper, we have presented an alternative approach to non-magnetic coordinate-transformation-based

invisibility cloaking. Unlike other approaches in the literature, the proposed strategy does not rely on approximate parameter reductions but rather on the design, via parametric optimization, of a *nearly-transparent* anisotropic and spatially inhomogeneous virtual domain, and is amenable to *exact analytic* treatment.

After derivation of the relevant analytic solutions, we have presented a body of representative parametric studies. Our results indicate that, when the unavoidable non-idealities (parameter truncations, losses, dispersion) of typical metamaterial implementations are taken into account, the overall performance attainable is comparable to that of a standard (magnetic) cloak.

The idea underlying the proposed strategy is rather general and, besides the cloaking scenarios, it may open up interesting perspectives for other transformation-optics applications, such as hyperlensing⁵³. In this framework, it should also be emphasized that the class of constitutive relationships in (1) represents only one example of nearly-transparent media amenable to analytic solutions, and exploration of further classes is certainly worth of interest and currently being pursued. In particular, configurations featuring a larger number of parameters may be utilized, together with more sophisticated optimization strategies, in order to achieve broadband or multi-band responses, and/or to enforce constraints in the variation ranges of the constitutive parameters of the transformation medium. Of particular interest are also the “masking” application scenarios^{54,55}, where one is interested in changing the scattering signature of an object (e.g., making it appear larger, smaller, or of different shape), and thus the desired scattering response is *inherently non-zero*. In such scenarios, the virtual-domain medium may offer extra degrees of freedom exploitable for the design of the desired scattering signature.

APPENDIX A: PERTAINING TO EQ. (22)

Particularizing the Helmholtz equation in (21) to the constitutive parameters in (1), we obtain

$$\left[\frac{d^2}{dr'^2} + \left(\frac{1+\gamma}{r'} + \frac{\alpha}{R_2} \right) \frac{d}{dr'} \right] \Psi_m(k_0 r') + \left[k_0^2(1-p) + \frac{pk_0^2 R_2}{r'} - \left(\frac{m}{r'} \right)^2 \right] \Psi_m(k_0 r') = 0, \quad (\text{A1})$$

which, letting $\tau = \xi r'$ [with ξ defined in (23b)], becomes

$$\left[\frac{d^2}{d\tau^2} + \left(\frac{\alpha}{\xi R_2} + \frac{1+\gamma}{\tau} \right) \frac{d}{d\tau} \right] \Psi_m\left(\frac{k_0 \tau}{\xi}\right) + \left[\frac{(1-p)k_0^2}{\xi^2} + \frac{pk_0^2 R_2}{\xi \tau} - \frac{m^2}{\tau^2} \right] \Psi_m\left(\frac{k_0 \tau}{\xi}\right) = 0. \quad (\text{A2})$$

and, via the mapping

$$\Psi_m\left(\frac{k_0 \tau}{\xi}\right) = \tau^{\frac{\nu m - \gamma}{2}} \exp\left[-\frac{(\xi R_2 + \alpha)\tau}{2\xi R_2}\right] \bar{\Psi}_m(\tau), \quad (\text{A3})$$

reduces to

$$\left\{ \tau \frac{d^2}{d\tau^2} + (1 + \nu_m - \tau) \frac{d}{d\tau} - \zeta_m \right\} \bar{\Psi}_m(\tau) = 0, \quad (\text{A4})$$

with ν_m and ζ_m defined in (23a) and (23c), respectively. Equation (A4) is readily recognized to be the Kummer equation [cf. Eq.(13.1.1) in Ref. 50], and admits two independent solutions in terms of confluent hypergeometric functions [cf. Eqs. (13.1.2), (13.1.3) in Ref. 50], from which the final solutions in (22) follow straightforwardly via inverse mapping. Note that, as a possible alternative route, the mapping

$$\Psi_m\left(\frac{k_0\tau}{\xi}\right) = \tau^{-\left(\frac{\gamma+1}{2}\right)} \exp\left(-\frac{\alpha\tau}{2\xi R_2}\right) \tilde{\Psi}_m(\tau) \quad (\text{A5})$$

would lead to the Whittaker equation [cf. Eq. (13.1.31) in Ref. 50].

APPENDIX B: PERTAINING TO THE APPROXIMATIONS IN (32)

We start recalling that, for $r' \rightarrow 0$, the wavefunctions $\Psi_m^{(1)}$ in (22) are regular, since $\nu_m \geq \gamma$ [cf. (23a)] and $M(\zeta_m, \nu_m + 1, 0) = 1$ [cf. Eq. (13.1.2) in Ref. 50], whereas $\Psi_m^{(2)}$ are singular, since [cf. Eq. (13.1.3) in Ref. 50]

$$U(\zeta_m, \nu_m + 1, \xi r') \sim -\frac{\pi(\xi r')^{-\nu_m}}{\sin[\pi(\nu_m + 1)]\Gamma(\zeta_m)\Gamma(1 - \nu_m)}, \quad r' \rightarrow 0, \quad (\text{B1})$$

where $\Gamma(\cdot)$ is the Gamma function [cf. Eq. (6.1.1) in Ref. 50]. We then define

$$\Delta' = f(R_1 + \Delta), \quad (\text{B2})$$

where, in view of (15a),

$$\Delta = g(\Delta') - R_1 \sim \frac{\exp(-\alpha)\chi R_2^{s-\gamma}}{R_1(\gamma - s + 2)} (\Delta')^{\gamma-s+2}. \quad (\text{B3})$$

Thus, combining (22), (B1) and (B2), we obtain

$$\Psi_m^{(1,2)}(k_0\Delta') \sim \varsigma_{1,2} \left(\frac{\Delta'}{R_2}\right)^{\frac{\pm\nu_m-\gamma}{2}}, \quad (\text{B4a})$$

$$\dot{\Psi}_m^{(1,2)}(k_0\Delta') \sim \varsigma_{1,2} \left(\frac{\pm\nu_m-\gamma}{2}\right) \left(\frac{\Delta'}{R_2}\right)^{\frac{\pm\nu_m-\gamma-2}{2}} \quad (\text{B4b})$$

where $\varsigma_{1,2}$ are irrelevant constants. Then, by recalling (30) and that

$$\dot{\psi}_m^{(1,2)}(k_0r) = \frac{\dot{\Psi}_m^{(1,2)}(k_0r')}{\dot{g}(r')}, \quad (\text{B5})$$

and substituting into (31), we obtain

$$d_m J_m(k_0 R_1) \sim a_m \varsigma_1 \left(\frac{\Delta'}{R_2}\right)^{\frac{\nu_m-\gamma}{2}} + b_m \varsigma_2 \left(\frac{\Delta'}{R_2}\right)^{\frac{-\nu_m-\gamma}{2}}, \quad (\text{B6a})$$

$$d_m \dot{J}_m(k_0 R_1) \sim \left(\frac{\Delta'}{R_2}\right)^{\gamma+1} \left[a_m \eta_1 \left(\frac{\Delta'}{R_2}\right)^{\frac{\nu_m-\gamma-2}{2}} + b_m \eta_2 \left(\frac{\Delta'}{R_2}\right)^{\frac{-\nu_m-\gamma-2}{2}} \right], \quad (\text{B6b})$$

where $\eta_{1,2}$ are other irrelevant constants. Equations (B6) can be readily solved with respect to b_m and d_m , yielding

$$b_m \sim a_m \left(\frac{\Delta'}{R_2}\right)^{\nu_m} \times \left[\frac{\eta_1 J_m(k_0 R_1) \left(\frac{\Delta'}{R_2}\right)^{\gamma} - \varsigma_1 \dot{J}_m(k_0 R_1)}{\varsigma_2 \dot{J}_m(k_0 R_1) - \eta_2 J_m(k_0 R_1) \left(\frac{\Delta'}{R_2}\right)^{\gamma}} \right], \quad (\text{B7a})$$

$$d_m \sim \frac{a_m (\eta_1 \varsigma_2 - \eta_2 \varsigma_1) \left(\frac{\Delta'}{R_2}\right)^{\frac{\gamma+\nu_m}{2}}}{\varsigma_2 \dot{J}_m(k_0 R_1) - \eta_2 J_m(k_0 R_1) \left(\frac{\Delta'}{R_2}\right)^{\gamma}}, \quad (\text{B7b})$$

from which, neglecting the higher-order terms in (Δ'/R_2) and recalling (B3), the approximations in (32) follow straightforwardly.

* Electronic address: vgaldi@unisannio.it

¹ W. K. Kahn and H. Kurss, *IEEE Trans. Antennas Propag.* **13** 671, 1965.

² M. Kerker, *J. Opt. Soc. Am.* **65**, 376 (1975).

³ H. Chew and M. Kerker, *J. Opt. Soc. Am.* **66**, 445 (1976).

⁴ N. G. Alexopoulos and U. K. Uzunoglu, *Appl. Opt.* **17**, 235 (1978).

- ⁵ P.-S. Kildal, A. Kishk, and A. Tenges, *IEEE Trans. Antennas Propagat.* **44**, 1509 (1996).
- ⁶ B. J. Hoenders, *J. Opt. Soc. Am. A* **14**, 262 (1997).
- ⁷ D. Schurig, J. J. Mock, B. J. Justice, S. A. Cummer, J. B. Pendry, A. F. Starr, and D. R. Smith, *Science* **314**, 977 (2006).
- ⁸ A. Alù and N. Engheta, *Phys. Rev. E* **72**, 016623 (2005).
- ⁹ M. G. Silveirinha, A. Alù, and N. Engheta, *Phys. Rev. E* **75**, 036603 (2007).
- ¹⁰ J. B. Pendry, D. Schurig, and D. R. Smith, *Science* **312**, 1780 (2006).
- ¹¹ U. Leonhardt and T. G. Philbin, *New J. Phys.* **8**, 247 (2006).
- ¹² U. Leonhardt, *Science* **312**, 1777 (2006).
- ¹³ D. Schurig, J. B. Pendry, and D. R. Smith, *Opt. Express* **14**, 9794 (2006).
- ¹⁴ I. I. Smolyaninov, Y. J. Hung, and C. C. Davis, *Opt. Lett.* **33**, 1342 (2008).
- ¹⁵ G. W. Milton and N. A. P. Nicorovici, *Proc. R. Soc. London A* **462**, 3027 (2006).
- ¹⁶ A. Hakansson, *Opt. Express* **15**, 4328 (2007).
- ¹⁷ P. Alitalo, O. Luukkonen, L. Jylha, J. Venermo, and S. A. Tretyakov, *IEEE Trans. Antennas Propagat.* **56**, 416 (2008).
- ¹⁸ A. Alù and N. Engheta, *J. Opt. A* **10**, 093002 (2008).
- ¹⁹ U. Leonhardt and D. R. Smith, *New J. Phys.* **10**, 115019 (2008).
- ²⁰ A. Greenleaf, Y. Kurylev, M. Lassas, and G. Uhlmann, *SIAM Rev.* **51**, 3 (2009).
- ²¹ A. Greenleaf, Y. Kurylev, M. Lassas, and G. Uhlmann, *Phys. Rev. Lett.* **99**, 183901 (2007).
- ²² H. Chen, X. Luo, H. Ma, and C. T. Chan, *Opt. Express* **16**, 14603 (2008).
- ²³ G. Castaldi, I. Gallina, V. Galdi, A. Alù, and N. Engheta, *Opt. Express* **17**, 3101 (2009).
- ²⁴ J. Li and J. B. Pendry, *Phys. Rev. Lett.* **101**, 203901 (2008).
- ²⁵ R. Liu, C. Ji, J. J. Mock, J. Y. Chin, T. J. Cui, and D. R. Smith, *Science* **323**, 366 (2009).
- ²⁶ L. H. Gabrielli, J. Cardenas, C. B. Poitras, and M. Lipson, arXiv:0904.3508v1 [physics.optics] (2009).
- ²⁷ J. Valentine, J. Li, T. Zentgraf, G. Bartal, and X. Zhang, arXiv:0904.3602v1 [physics.optics] (2009).
- ²⁸ Y. Lai, H. Chen, Z.-Q. Zhang, and C. T. Chan, *Phys. Rev. Lett.* **102**, 093901 (2009).
- ²⁹ H. Ma, S. Qu, Z. Xu, and J. Wang, *Appl. Phys. Lett.* **94**, 103501 (2009).
- ³⁰ S. A. Cummer and D. Schurig, *New J. Phys.* **9**, 45 (2007).
- ³¹ J. B. Pendry and J. Li, *New J. Phys.* **10**, 115032 (2008).
- ³² G. W. Milton, M. Briane, and J. R. Willis, *New J. Phys.* **8**, 248 (2006).
- ³³ S. Zhang, D. A. Genov, C. Sun, and X. Zhang, *Phys. Rev. Lett.* **100**, 123002 (2008).
- ³⁴ S. A. Cummer, B.-I. Popa, D. Schurig, D. R. Smith, and J. Pendry, *Phys. Rev. E* **74**, 036621 (2006).
- ³⁵ B. Zhang, H. S. Chen, B. I. Wu, Y. Luo, L. X. Ran, and J. A. Kong, *Phys. Rev. B* **76**, 121101 (2007).
- ³⁶ Z. Ruan, M. Yan, C. W. Neff, and M. Qiu, *Phys. Rev. Lett.* **99**, 113903 (2007).
- ³⁷ H. S. Chen, B. I. Wu, B. Zhang, and J. A. Kong, *Phys. Rev. Lett.* **99**, 063903 (2007).
- ³⁸ H. Y. Chen, Z. X. Liang, P. J. Yao, X. Y. Jiang, H. R. Ma, and C. T. Chan, *Phys. Rev. B* **76**, 241104 (2007).
- ³⁹ P. J. Yao, Z. X. Liang, and X. Y. Jiang, *Appl. Phys. Lett.* **92**, 031111 (2008).
- ⁴⁰ M. Yan, Z. C. Ruan, and M. Qiu, *Phys. Rev. Lett.* **99**, 233901 (2007).
- ⁴¹ H. Tao, N. I. Landy, K. Fan, A. Strikwerda, W. J. Padilla, R. D. Averitt, and X. Zhang, Proc. 2008 Int. Electron Devices Meeting (IEDM '08), San Francisco, CA, USA, Dec. 15-17, 2008, pp. 11.6.1-11.6.4.
- ⁴² J. Zhou, Th. Koschny, M. Kafesaki, E. N. Economou, J. B. Pendry, and C. M. Soukoulis, *Phys. Rev. Lett.* **95**, 223902 (2005).
- ⁴³ W. S. Cai, U. K. Chettiar, A. V. Kildishev, and V. M. Shalaev, *Nature Photonics* **1**, 224 (2007).
- ⁴⁴ W. Cai, U. K. Chettiar, A. V. Kildishev, V. M. Shalaev, and G. W. Milton, *Appl. Phys. Lett.* **91**, 111105 (2007).
- ⁴⁵ W. Cai, U. K. Chettiar, A. V. Kildishev, and V. M. Shalaev, *Opt. Express* **16**, 5444 (2008).
- ⁴⁶ I. Gallina, G. Castaldi, and V. Galdi, *Microwave Opt. Technol. Lett.* **50**, 3186 (2008).
- ⁴⁷ L. Zhang, M. Yan, and M. Qiu, *J. Opt. A* **10**, 5 (2008).
- ⁴⁸ Z. Jacob and E. E. Narimanov, *Opt. Express* **16**, 4597 (2008).
- ⁴⁹ Y. Luo, J. Zhang, H. Chen, S. Xi, and B.-I. Wu, *Appl. Phys. Lett.* **93**, 033504 (2008).
- ⁵⁰ M. Abramowitz and I. A. Stegun, *Handbook of Mathematical Functions* (Dover, New York, 1964).
- ⁵¹ Obviously, the scattering width in (33) admits a trivial (zero-valued) global minimum for $\alpha = \gamma = p = 0$ [for which the virtual-domain medium in (1) reduces to vacuum], which is, however, incompatible with the assumed constraints.
- ⁵² Note that, in view of the different expressions, identical truncation parameters Δ/R_1 in (12) and (34) would yield different variation ranges of the constitutive parameters. In order to guarantee a meaningful comparison, the value of Δ/R_1 reported in the graphs is referred to (34), and the one pertaining to (12) is adjusted accordingly so as to yield comparable (within a $\pm 10\%$ window) variation ranges of the permittivities.
- ⁵³ A. V. Kildishev and E. E. Narimanov, *Opt. Lett.* **32**, 3432 (2007).
- ⁵⁴ F. L. Teixeira, *Microwave Opt. Technol. Lett.* **49**, 2051 (2007).
- ⁵⁵ O. Ozgun and M. Kuzuoglu, *Microwave Opt. Technol. Lett.* **49**, 2386 (2007).